Applications of the new magnetostatic solver/ AMS preconditioner in LS-DYNA®

Miro Duhovic[1], Inaki Caldichoury[2], Pierre L'Eplattenier[2], Trang Nguyen[2], Joachim Hausmann[1], Lars Kielhorn[3], Thomas Rüberg[3], Jürgen Zechner[3]

[1]Leibniz-Institut für Verbundwerkstoffe GmbH, Technische Universität Kaiserslautern, Erwin-Schrödinger-Straße 58, 67663 Kaiserslautern, Germany
[2]Ansys - Livermore Software Technology LLC, 7374 Las Positas Road, Livermore, CA 94551, USA
[3]Tailsit, Nikolaipl. 4, 8020 Graz, Austria

Abstract

Previous implementations of LS-DYNA's EM module have relied on an explicit scheme, requiring very small time-step sizes and therefore long simulation times. Recently, a new magnetostatic solver/ AMS preconditioner has been developed in LS-DYNA®. Unlike the current implementation, the new solver is unconditionally stable with respect to the time-step size and allows for the handling of materials with high permeability and low electrical conductivity. In this paper, the capabilities of the new solver is tested on the use-case of carbon fiber reinforced thermoplastic composite (CFRTPC) laminate induction heating using magnetic flux concentrators/field formers. In the current work, induction heating characterization experiments were performed on carbon fiber poly(ether ether ketone) (CF/PEEK) laminates using two different coil geometries. Temperature measurements for both the heating and cooling cycles were recorded using two laser guided non-contact pyrometers on both sides of the plate specimens at specific locations depending on the coil geometry. In addition, full infrared thermal imagery was recorded for the non-coil side of the specimen. The influence of the coil's magnetic flux concentrators was also studied to see if the effect of magnetic flux concentration could be simulated in LS-DYNA®. Two different shaped induction coils (a figure 8 and a single turn square section coil) with and without magnetic flux concentrators are used to demonstrate the enhanced functionality of the new solver. In addition, a second application involving induction heating CFRTPC UD-laminates, previously not possible with the standard electromagnetic solver, is also demonstrated.

1 Introduction

The continuous induction welding of CFRTPC materials usually involves complexly shaped inductor geometries in order to generate the desired heating pattern at the joining interface [1-3]. In addition, the CFRTPC material itself usually consists of multiple layers of unidirectional (UD) plies built-up in different orientations into a laminate, optimized for the specific load case applied to the part [4]. The development of finite element models for induction welding simulations of CFRTPCs involves the detailed modelling of both these aspects of the system, which has now been enabled by a new EM solver approach [5].

1.1 Induction coils and flux concentrators

Induction coils (or inductors) are fabricated from circular or square section copper tubing and these days
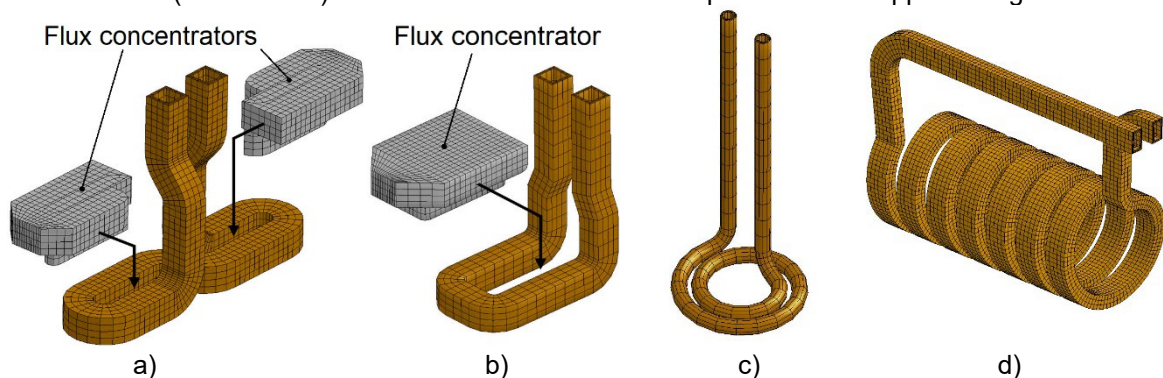
Fig.1: *Various coil designs available at the Leibniz-Institut für Verbundwerkstoffe GmbH, Germany applied for the inductive heating and welding of polymer composites – a) Figure 8 coil with flux concentrators, b) single turn coil with flux concentrator, c) "pancake" coil, and d) helical coil.*

can even be 3D printed via selective laser sintering. A selection of the different induction coil geometries, used at the Leibniz-Institut für Verbundwerkstoffe GmbH is shown Figure 1.

In addition to the (copper) coil itself, so called magnetic "flux concentrators" or "field formers" can also be used (see Figure 1 a) and b)). A flux concentrator is made from ferrous material and is used to direct or intensify the magnetic field of an induction coil towards a desired location. Such materials are typically used in induction heating systems in order to improve the overall energy efficiency of the process. Flux concentrators are made from soft magnetic (iron based) materials, are easily machinable (even soft moldable forms exist) and possess the following material properties:

- high magnetic permeability
- low electrical conductivity (which reduces eddy current losses)
- high thermal conductivity (which reduces local heating)
- low thermal expansion

Figure 2 shows the effect a flux concentrator has on the magnetic field, which exists around an induction coil. As the relative magnetic permeability of a flux concentrator can be 1-2 orders of magnitude higher than air, the magnetic field prefers to pass through the flux concentrator rather than the surrounding air. The flux concentrators used in this work have been sourced from the company Fluxtrol®. A wealth of information, including detailed material properties (e.g. BH curves) for many different types of commercially available flux concentrator materials can be found on their website [6].
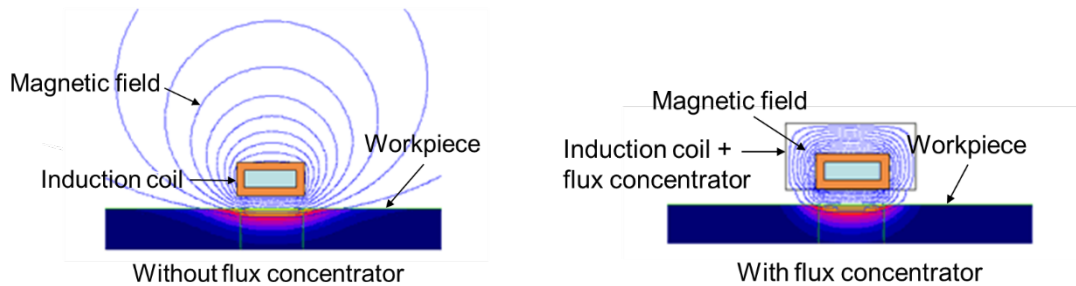
Fig.2: Schematic showing the effect of a flux concentrator on the magnetic field around an induction coil [6].

1.2 Laminate structures

Laminate structures based on unidirectional plies and their customizable configuration forms the fundamental basis for composite design, tailorability and part optimization. Figure 3 shows some basic examples of different quasi-isotropic laminate configurations along with their terminology. Figures 3 b) and c) show examples of symmetric and asymmetric laminate configurations respectively. There are however endless combinations, which depends on the structural design requirements. The angles at which the individual layers can be assigned can be anything from 0° to -89°. With respect to induction heating/welding, this means that each laminate has its own unique heating behavior. The ability to simulate the induction heating behavior of such laminates rather than characterize each one individually is therefore very important.
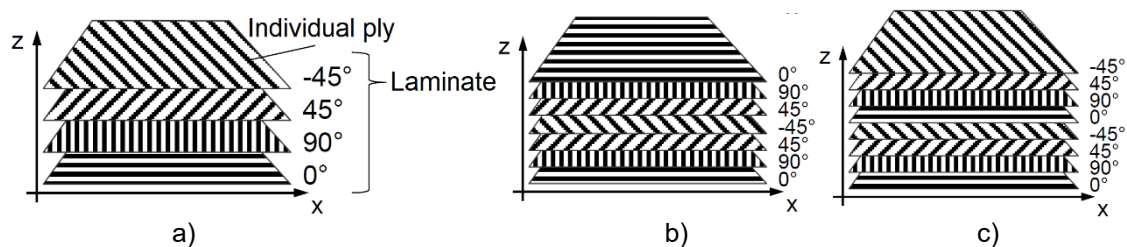
Fig.3: Some basic examples of different possible laminate structures and their associated terminology, a) [0 / 90 / 45 / -45], b) [0 / 90 / 45 / <u>-45</u>]$_s$ and c) [0 / 90 / 45 / -45]$_2$.

2 Application 1: Simulating the effects of magnetic flux concentrators

2.1 Equipment and materials

The material used in the characterization study was pre-consolidated TohoTenax CF/PEEK laminate (TPCL PEEK-HTA40) with a thickness of 2.17 mm. The laminate is produced from 7 plies of the material which uses a 5H-satin weave reinforcement. The recommended processing temperature and pressure are 380°C – 420°C and 8 – 15 bars respectively. For the purposes of the present static heating tests, the heating safety cut-off temperature was set to 360°C to avoid any overheating and burning of the material specimens. This was done using a third pyrometer connected to the induction heating generator unit pointed in the same position as the pyrometer recording the temperatures on the coil side of the specimen setup.

A Hüttinger Elektronik TruHeat HF 5010 generator available at the IVW (see Figure 4) was used together with an 8:1 transformer. Some initial testing of the equipment was performed in order to obtain an idea for the range of settings possible using the 8:1 transformer. The transformer unit contains two sets of interchangeable capacitor slots allowing the wider variation of frequency. The total range of capacitor sets available is between 0.1uF and 2.4uF and a table showing a summary of the generator readings for both the figure 8 and single turn coils for different capacitor arrangements in the transformer unit is shown in Tables 1 and 2. It must be noted that for different specimens (material type, thickness, coupling distance etc.) that the capacitors used to give a desired set of induction parameters will be different. This is because all of the aforementioned parameters are involved in determining the electromagnetic circuit. However, since the coil geometry and size are a major influence, a rough idea of the capacitor set which needs to be used can be obtained by testing the coils in the absence of a heating specimen.
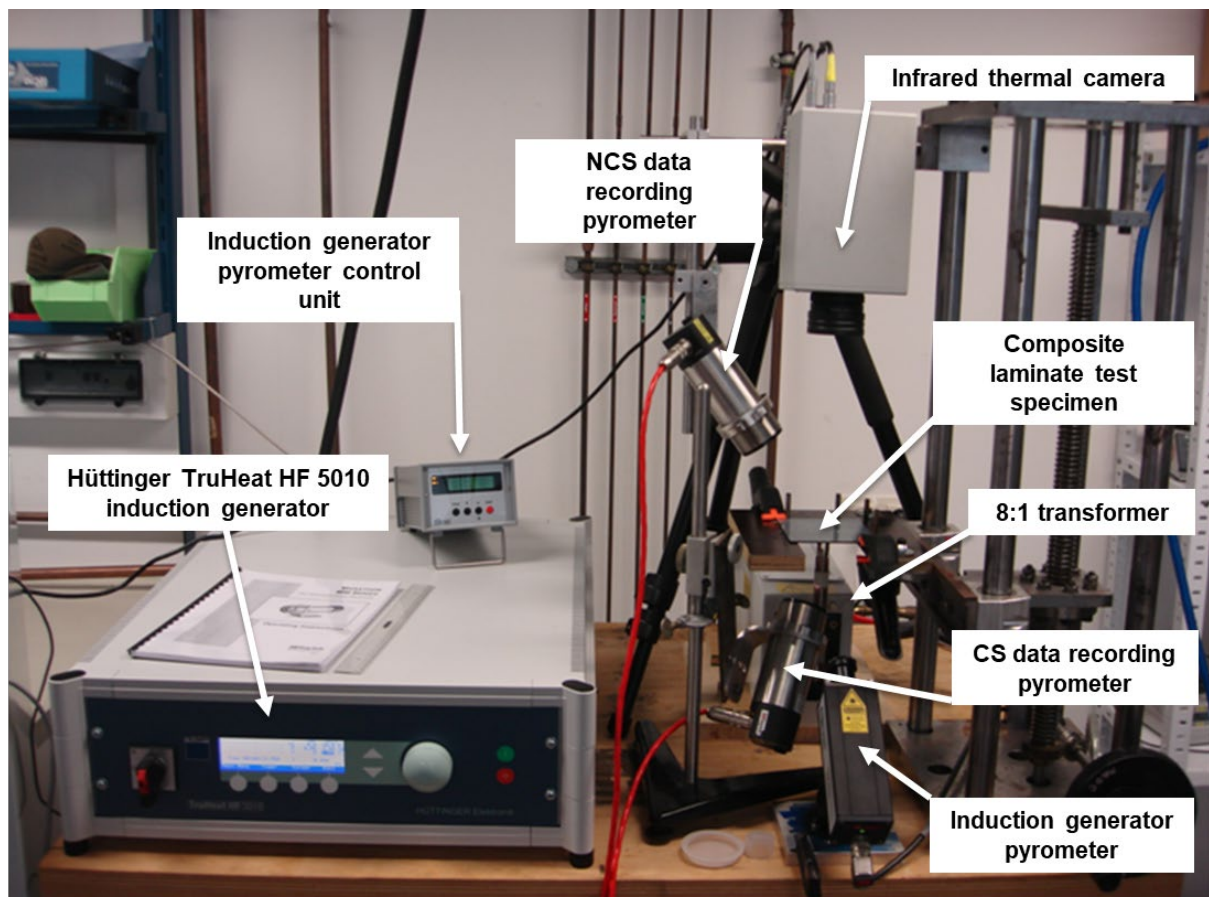
Fig.4: Induction heating characterization equipment available at the Leibniz-Institut für Verbundwerkstoffe GmbH, Germany.

Figure 8 Coil	Capacitor Configuration (uF)				Max. Power (kW)	Frequency (kHz)	Current (A)	Voltage (V)
	C1	C2	C3	C4	2.30	336	35	117
Water flowrate (litres/min)								
2.7	2.4	-	2.4	-				
Note:	Can be adjusted up to 550kHz at reduced power							
	C1	C2	C3	C4	2.62	546	32.5	194
	0.5	0.33	0.5	0.33				
Note:	Frequency can be adjusted at reduced power							
	C1	C2	C3	C4	2.30	600	30	238
	0.5	0.17	0.5	0.17				
Note:	Can be adjusted up to 650kHz at reduced power (1.26kW, 18.8A, 136V)							
	C1	C2	C3	C4	2.20	633	28.9	171
	0.5	0.1	0.5	0.1				
Note:	Can be adjusted up to 650kHz at reduced power (1.66kW, 23.5A, 117V)							
	C1	C2	C3	C4	0.61	864	9.9	61
	0.5	-	0.5	-				
Note:	Cannot be adjusted any further							
	C1	C2	C3	C4	1.52	768	21.4	191
	0.33	0.1	0.33	0.1				
Note:	Cannot be adjusted any further							
Note 2:	Capacitor configurations of 0.33uF, 0.27uF and 0.1uF all do not work with this coil (result in frequencies above 1000kHz)							
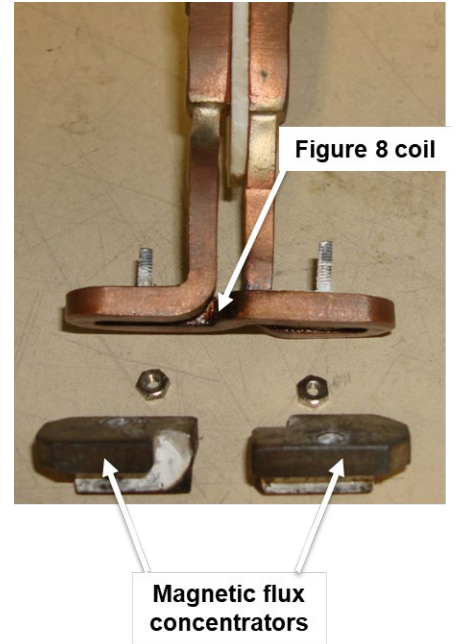
Table 1: Generator readings for different capacitor sets in the 8:1 transformer unit in the absence of any heating specimen (figure 8 inductor).

Single Turn Coil	Capacitor Configuration (uF)				Max. Power (kW)	Frequency (kHz)	Current (A)	Voltage (V)
	C1	C2	C3	C4	2.30	345	35.0	108
Water flowrate (litres/min)								
2.4	2.4	-	2.4	-				
Note:	Frequency can be adjusted higher at reduced power							
	C1	C2	C3	C4	2.29	570	29.9	172
	0.5	0.33	0.5	0.33				
Note:	Frequency can be adjusted higher at reduced power							
	C1	C2	C3	C4	2.30	619	29.6	247
	0.5	0.17	0.5	0.17				
Note:	Can be adjusted up to 650kHz at reduced power (1.50kW, 20.1A, 136V)							
	C1	C2	C3	C4	0.64	875	9.9	81
	0.5	0.1	0.5	0.1				
Note:	Cannot be adjusted any further							
	C1	C2	C3	C4	0.75	856	11.0	80
	0.5	-	0.5	-				
Note:	Cannot be adjusted any further							
	C1	C2	C3	C4	1.52	793	20.9	314
	0.33	0.1	0.33	0.1				
Note:	Cannot be adjusted any further							
	C1	C2	C3	C4	1.00	909	15.0	136
	0.33	-	0.33	-				
Note:	Cannot be adjusted any further							
Note 2:	Capacitor configurations of 0.27uF and 0.1uF all do not work with this coil (result in frequencies above 1000kHz)							
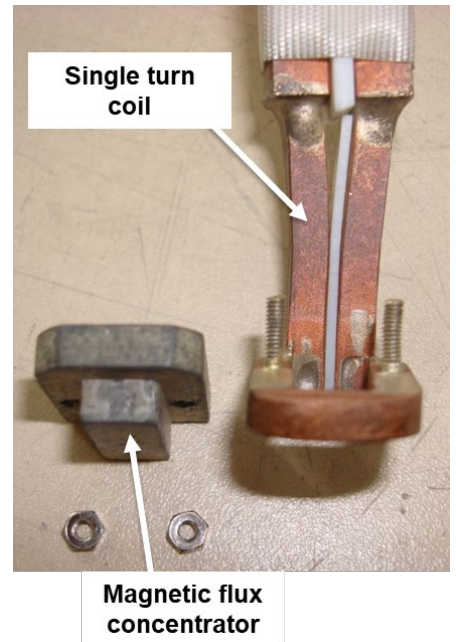
Table 2: Generator readings for different capacitor sets in the 8:1 transformer unit in the absence of any heating specimen (single turn inductor).

The target induction generator settings were **f = 650kHz, I = 20A (160A), P = 2.4kW** as used on previous equipment which was found to give suitable conditions for welding CF/PEEK. In order to allow these settings and given the results presented in Tables 1 and 2, it was suggested that the 0.67uF capacitor configuration should be used in IVW's 8:1 transformer unit for all the experiments. It should be noted that the actual current applied to the inductor is equal to the current value displayed on the generator multiplied by the transformer ratio (8). Therefore this is the current value which should be input into the `*EM_CIRCUIT` keyword using "circType 11" in the simulations. The frequency is the same as the value displayed on the generator converted to the respective unit system of the simulation model (usually Hz if SI units have been used).

2.2 Experimental details

2.3 Influence of coil and specimen type on generator settings

The single turn coil experiments were performed using a capacitor arrangement yielding 0.83uF in the 8:1 transformer rather than the 0.67uF that was found to be suitable during preliminary testing of the coils in the absence of any specimens as presented in Section 2.1. For the single turn coil it was found that in the absence of any specimen, a 0.67uF capacitor arrangement gave a maximum power setting of f = 618kHz, I = 29.5A, V = 234V, P = 2.20kW, while simply adding the single plate CF/PEEK specimen caused these settings to switch over to f = 878kHz, I = 9.0A, V = 49V, P = 0.64kW. Again, as mentioned in Section 2.1, the reason for this is due to the fact that all elements of the setup including the specimen and the flux concentrators have an influence on the final electromagnetic circuit that is created. Using the 0.83uF capacitor arrangement, a more stable set of generator settings were achieved with and without the specimen involved in the electromagnetic circuit. The final settings used for the single turn coil gave f = 608 kHz, I = 20.9 A, V = 167 V, P = 1.53 kW and f = 606 kHz, I = 20.9A, V = 170 V, P = 1.27 kW with and without the single plate CF/PEEK specimen respectively. For the single turn coil, during actual testing, it was not possible to maintain the desired power and frequency when running the experiments with and without a flux concentrator. This is the reason why the inputs for the single turn coil parameters (frequency, current, voltage and power) are quite different. For the figure 8 coil it was possible to maintain a relatively constant frequency, current, voltage and power with and without flux concentrators.

2.4 Single laminate heating with and without flux concentrators

The testing program involved both coil types and 100 x 100 x 2.17 mm thick CF/PEEK plate specimens. The tests ran over a time span of between 60 seconds (figure 8 inductor) and 120 seconds (single turn inductor) and both the heating and cooling characteristics for both inductor setups was recorded. The settings on the induction generator unit were kept as close as possible to experimentally validated plausible welding parameters (f = 650kHz, I = 21A, P = 2.4kW) and were documented for each test. The coupling distance of each coil to the laminate surface was kept constant at 2.1 mm for both coils and all the experiments. For both the figure 8 and single turn induction coils, a single point temperature profile was recorded using two pyrometers, coil side (CS) and non-coil side (NCS) on the laminate at the closest visible point to the center of the induction coil and the plate specimen. On the NCS, thermal imaging data was recorded using an infrared thermal camera. Figure 5 shows the location of pyrometer temperature measurements made on the CS of the specimen for both inductor types.
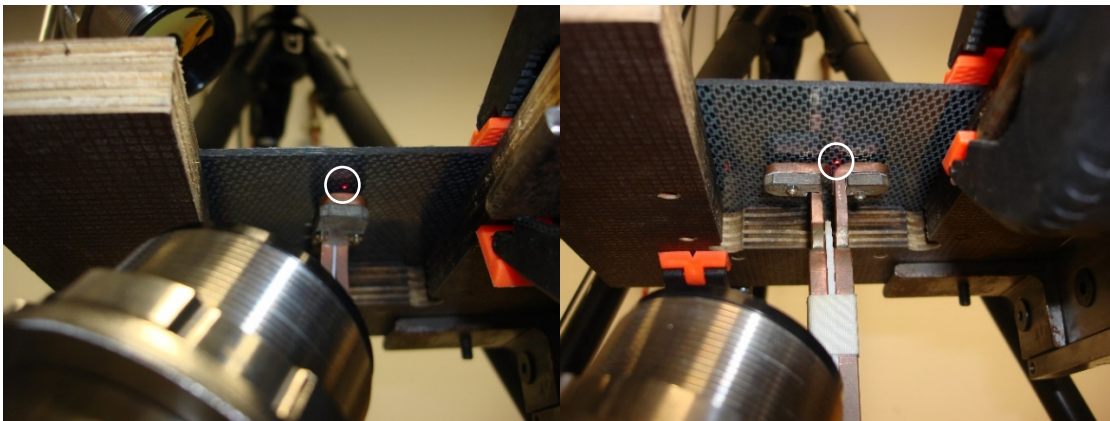
Fig.5: Locations of the pyrometer temperature measurement in the test setup using the single turn (left) and figure 8 coil (right).

Care was taken to place the laminate specimens in the same orientation in each of the tests to avoid any difference in the heating pattern due to the reinforcement structure in the CF/PEEK laminate. Contrary to metals and other isotropic materials, the heating pattern in laminated woven or UD CF/PEEK sheets has been shown to be generated mostly via the eddy current loops, which form due to the yarn cross-overs in the woven or laminated UD reinforcement structure [4].

2.4.1 Material properties

A summary of the main material properties used in the simulations is given below in Table 3. In addition, only a simple constant boundary convection (`*BOUNDARY_CONVECTION_SET`) of 5W/m^2.K was applied to the surfaces of the CF/PEEK laminate. More complex temperature dependent (vertical/horizontal) boundary convection and radiation via `*BOUNDARY_RADIATION_SET` can also be applied but was not done so in the present study to keep things simple.

Material Property		Air	Copper (Coil)	Flux Concentrator (FLUXTROL50)	CF/PEEK
Density (kg/m^3)		1.293	8960	6100	1790
Heat Capacity at (const. pressure) (J/(kg*K)		1010	385	[2]450	[4]1803
Thermal Conductivity (W/m*K)	k_1	0.026	390	6	[5]2.5
	k_2	-	-	-	[5]2.5
	k_3	-	-	-	[5]0.3
Electrical Conductivity (S/m)		1	[1]5.998 x 10^7	0.2	[6]2.500 x 10^4
Relative Permittivity		1	1	1	[7]3.7
Relative Permeability		1	1	[3]27.5-55	1
Surface Emissivity		-	0.5	-	-

[1]Constant electrical conductivity behavior implemented for the copper coil, therefore no change with respect to temperature
[2]Constant heat capacity of Iron at 25°C used
[3]Constant values taken from the Fluxtrol® website [6], non-constant relative permeability, ideally defined by a B-H curve
[4]Material property value taken from the IVW PhD thesis of Khan [7]
[5, 7]Material property values taken from the IVW PhD thesis of Moser [8]
[6] Electrical conductivity values taken from the work of Hoffmann [4]

Table 3: Summary of material properties used in the induction heating simulations.

2.4.2 Single turn coil

The results of the testing using the single turn coil were complicated due to the reasons discussed in Section 2.3. With this inductor, there is a very large difference in the heating rate with and without the use of flux concentrators making it difficult to find stable equivalent generator settings. As mentioned in Section 2.3, the settings used for the single turn coil were **f = 608 kHz, I = 20.9 A, V = 167 V, P = 1.53 kW** for the test case when using the flux concentrators and **f = 880kHz, I = 8.9 A, V = 36 V, P = 0.57 kW** (much lower power) for the test case without.

The difference in power is partly why the graph shown in Figure 6 shows a more aggressive heating curve, although in reality the single turn coil using flux concentrators is known to be a more aggressive heater than the figure 8 coil at the same power settings. Nevertheless, the tests provide at least some data for characterization of the finite element models although the generators settings were not able to be kept the same. If the graph presented in Figure 6 was considered over a much longer time period, (200 seconds), then a jump in the heating curves was observed for the tests performed without the flux concentrators. These jumps in temperature correspond to a change in the generator settings which switched from **f = 880kHz, I = 8.9 A, V = 36 V, P = 0.57 kW** to **f = 629kHz, I = 20.9 A, V = 137 V, P = 1.36 kW.** This event seemed to occur consistently upon the material reaching a temperature of approximately 230°C. It can only be speculated that something to do with the heating process causes a change in the material properties which in turn disturbs the stability of the electromagnetic circuit created. It should be noted that the capacitor set giving 0.83uF was used in the single turn coil test as the 0.67uF configuration was not stable, even in the case where the flux concentrators were used.

The heating patterns for the single turn coil up to the cut-off temperature are given in Figure 6. In these tests, the pyrometer laser spot was positioned so that the temperature measurements made by both pyrometers (CS and NCS) were at the hottest locations on the laminate under the coil. For the single turn coil placed perfectly parallel to the laminate specimen, this should be near the two corners at the front turn of the coil. Figure 5 (right) shows the exact location of the pyrometer temperature measurement. Unfortunately the single turn coil was not perfectly parallel resulting in slightly distorted thermal images, which would otherwise be expected to be perfectly symmetrical (see Figure 6).
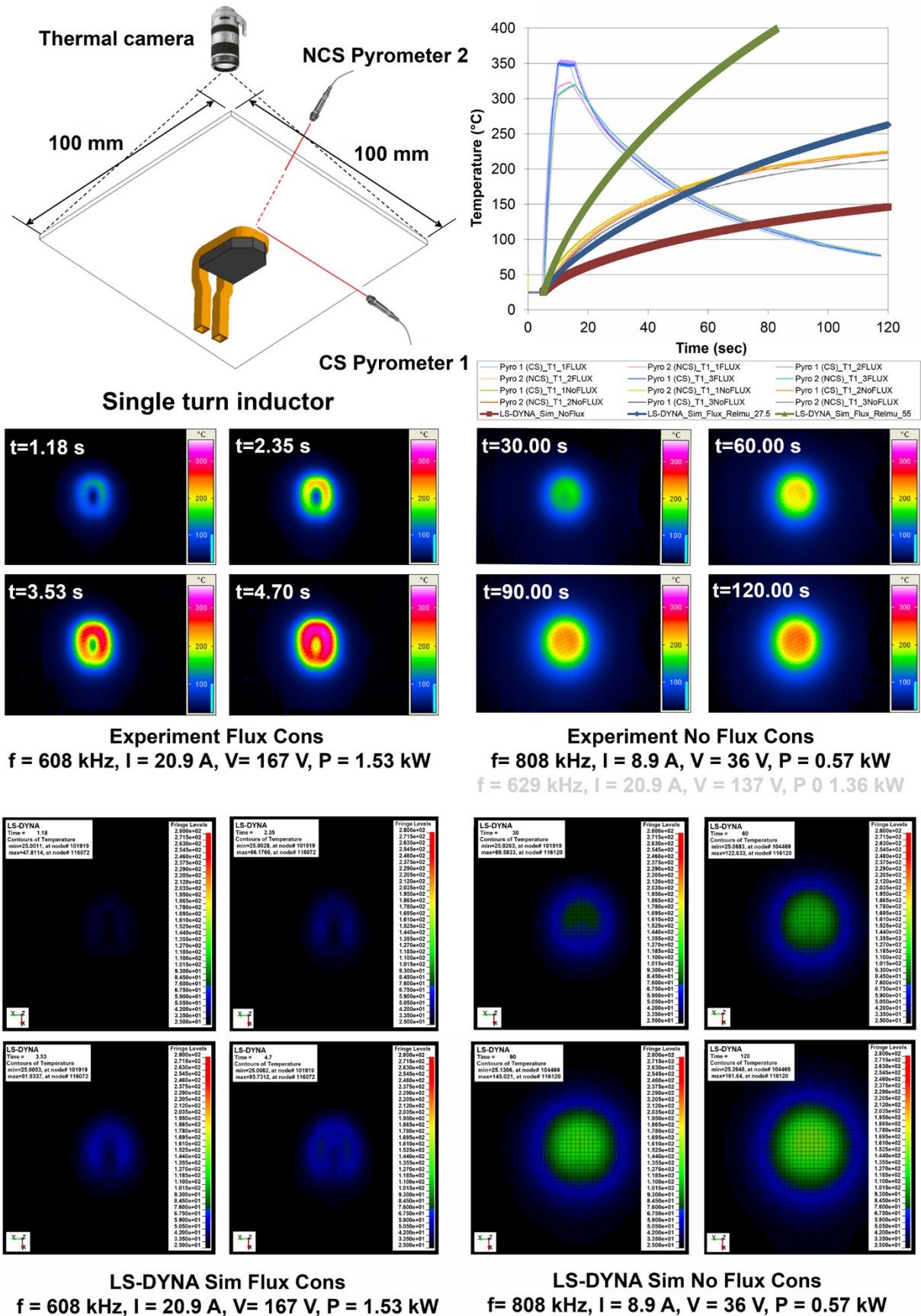
Fig.6: *Experimental results and LS-DYNA® simulations for the induction heating using the single turn inductor with and without flux concentrators.*

Nevertheless, a good idea of the heating pattern can still be obtained and be used for verification to some extent of the finite element models. Figure 6 also shows the heating patterns at very low heating rates for the single turn coil without its flux concentrators. Again, it should be noted that the induction generator settings were not stable enough to allow direct experimental comparisons of the heating patterns with equal generator settings (as could be done to some extent for the figure 8 coil, see subsequent section 2.4.3) with and without the flux concentrators. However, useful visualization of the influence of a low heating rate can be seen and used to compare with simulation models. The simulations show a good overall qualitative prediction, however the developed temperatures in the CFRTPC laminate both with and without flux concentrators seems to be highly under predicted.

2.4.3 Figure 8 coil

Figure 7 shows the pyrometer readings made at the center of the specimen for the figure 8 coil on both sides of the plate with and without the use of its flux concentrators. The experiment was performed three times for a given configuration and showed very repeatable results. For these experiments the generator unit was set to 2.4kW, 30A, 1400V, while the actual steady state generator settings that were recorded during the test were stable at **f = 601 kHz, I = 29.9 A, V = 167 V, P = 2.32 kW** for the case of the figure 8 coil using the flux concentrators and **f = 637 kHz, I = 28.9 A, V = 193 V, P = 2.23 kW** for the case without. It can be seen from the curves that when the figure 8 coil uses its flux concentrators the temperature on the CS reaches 360°C in approximately 3.5 seconds, while 35 seconds is required to reach the same temperature without the use of the flux concentrators. As can be expected, the difference in temperatures at the same planar location on both sides of the specimen is larger, approximately 90°C, when using flux concentrators compared to roughly 30°C when not using the flux concentrators due to the poor through thickness thermal conductivity of the material.

The results highlight the fact that attention needs to be paid to the heating rate, as heating the specimen longer as opposed to shorter by using different power settings on the induction generator, will give a different temperature at the joining interface also. As mentioned before, the NCS of the single plate specimen was monitored using an infrared thermal imaging camera. Figure 7 shows the development of the heating pattern at t = 0.875, 1.75, 2.625 and 3.5 seconds for the single laminate specimen. It can be seen that the highest temperature occurs at the symmetrical center of the coil geometry and exhibits a sharp s-shaped heating contour. Figure 7 also shows the development of the heating pattern at t = 8.75, 17.5, 26.25 and 35 seconds for the single laminate specimen without the use of flux concentrators. Note that the times referred to for the thermal images are the times taken from the start of heating, while those referred to in pyrometer graph are shown from the start of the experiment. The simulation curves are therefore shifted to the time that actual heating begins. This should be considered if exact time comparisons are made between the pyrometer reading and the thermal images.

Again, it is clear from the thermal images that the hottest part of the laminate occurs at the center of the laminate directly below the inflection point of the figure 8 coil geometry. However, the effects of the slower heating rate can be seen on the temperature distribution in the CF/PEEK laminate. The s-shaped temperature contour is now only just present at the final target temperature and is more evenly distributed than in the case of the coil using the flux concentrators where the heating rate is much higher. This effect can become very important when choosing the speed at which the coil can move during the induction welding procedure. For example, it cannot be assumed that to move the coil faster, simply a larger heat input rate, or power to the coil is required. In this case, the temperature of the surface closest to the coil will be far too high. The required heating pattern at the joining interface therefore becomes smaller, less uniform and highly dependent on the induction coil geometry. The simulations show a good overall quantitative and qualitative prediction, even when the developed temperature with and without flux concentrators is slightly under predicted.

In general, the simulation results for both coils predict a much lower effectiveness of the flux concentrators compared to that seen in the experiments. This is more apparent in the case of the single turn coil. As shown in Figure 1 a) and b), the figure 8 coil consists of a much finer mesh than the single turn coil, which is likely the main reason why the single turn coil results deviate more. Care should therefore be taken to mesh the coil and the flux concentrator to a satisfactory resolution, in particular for aggressively heating inductors. Another reason for the lower predicted effect of the flux concentrators could also be the simplified constant values (27.5 and 55) of relative magnetic permeability used. In the future, better prediction accuracy is expected if BH curves can be applied. In addition, it can also be seen on the Fluxtrol® website, that many of the materials possess directional magnetic permeability properties due to processing. This would be another great feature to include into `*EM_MAT_002`.
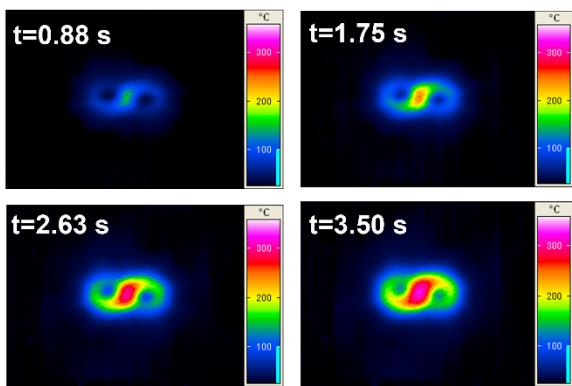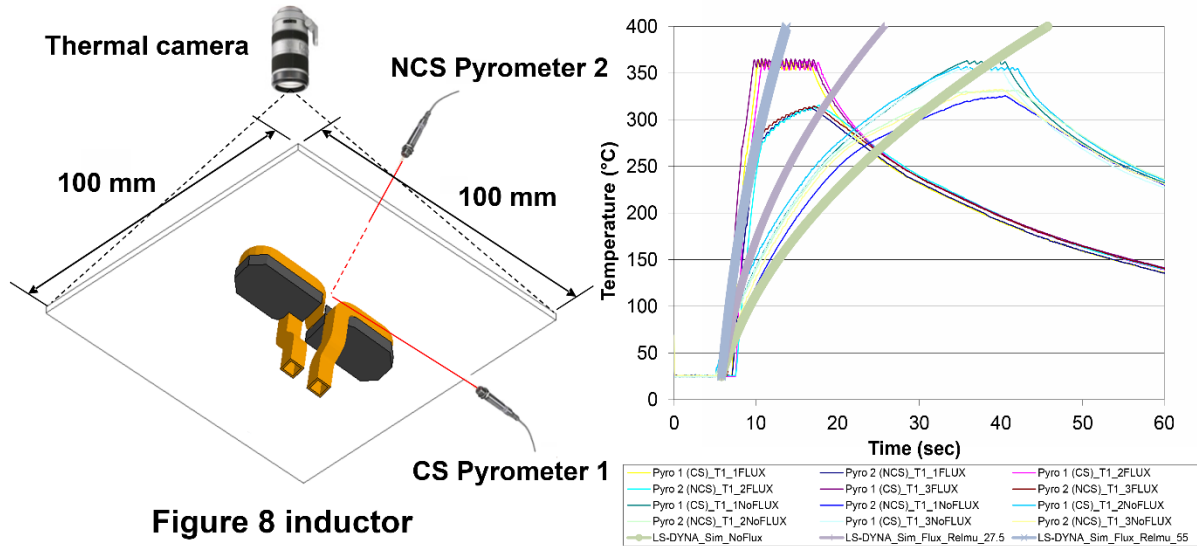
Figure 8 inductor

Experiment Flux Cons
f = 601 kHz, I = 29.9 A, V= 167 V, P = 2.32 kW

Experiment No Flux Cons
f = 637 kHz, I = 28.9 A, V = 193 V, P = 2.23 kW
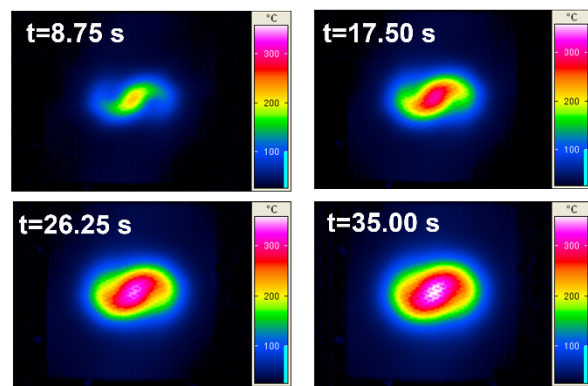
LS-DYNA Sim Flux Cons
f = 601 kHz, I = 29.9 A, V= 167 V, P = 2.32 kW
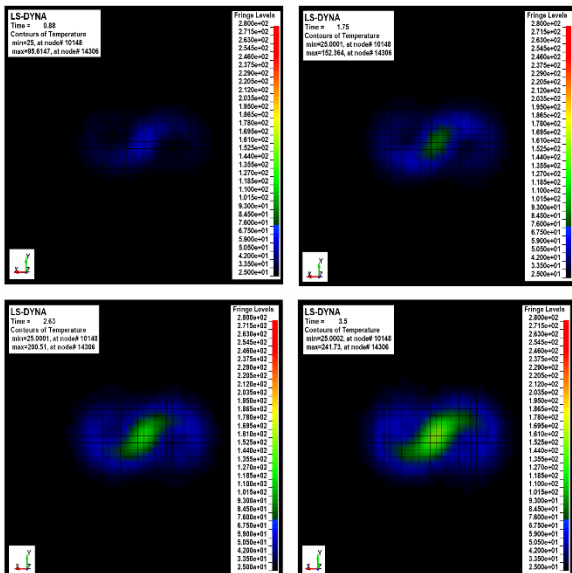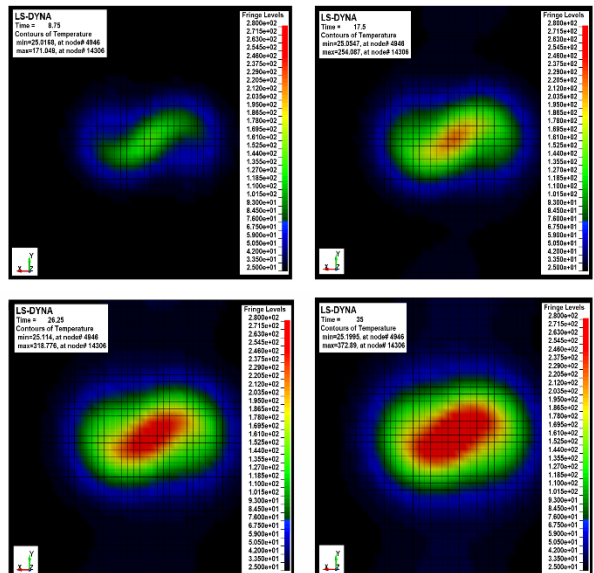
LS-DYNA Sim No Flux Cons
f= 637 kHz, I = 28.9 A, V = 193 V, P = 2.23 kW

Fig.7: *Experimental results and LS-DYNA® simulations for the induction heating using the figure 8 inductor with and without flux concentrators.*

3 Application 2: Simulating UD-Laminate heating behaviour

In the work of Hoffmann et al. [5], an analytical model describing the inductive heating behavior of carbon fiber reinforced thermoplastic composite (CFRTPC) laminates was created and implemented in LS-DYNA®. The model allows the precise definition of anisotropic electrical conductivity material parameters as well as anisotropic thermal properties defined through micromechanical considerations and constituent (fiber and matrix) material properties. Detailed investigations of the through thickness temperature distribution as well as the distribution of the electric current density in various location of the laminate could be carried out. However, for certain laminate configurations where the laminate configuration leads to very low and highly anisotropic electrical conductivity parameters, the standard electromagnetic solver encounters convergence problems.

In this section, we once again investigate how the angle difference of the individual plies qualitatively and quantitatively affects the heating behavior of a CFRTPC laminate. To investigate the influence of ply orientation, the angular difference of the plies is changed in 10° steps from $(0/90)_{10}$ to $(0/10)_{10}$ (see Figure 16). With an angular difference of 0° between the UD-layers in the laminate, i.e. a purely unidirectional structure, practically no heating of the laminate would be expected. For this study, the parameters listed in Table 4 were used.
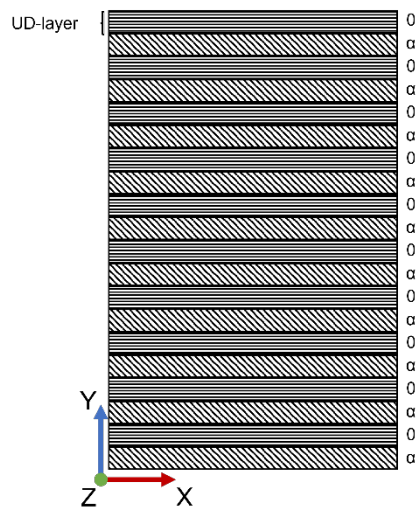
Fig.8:   Schematic representation of the layer structures used for the investigation of the influence of the layer orientation on the laminate heating behavior.

Parameter	Value
$\hat{I}$ in A	297.5
f in MHz	490
V_f	0.5
t_{LAM} in mm	2
Layer configuration	$(0/90)_{10}$, $(0/+80)_{10}$, $(0/+70)_{10}$, $(0/+60)_{10}$, $(0/+50)_{10}$, **$(0/+40)_{10}$, $(0/+30)_{10}$, $(0/+20)_{10}$, $(0/+10)_{10}$**
Stop criteria	Simulation time 5 sec

Table 4:   Simulation parameters used for the investigation of the influence of ply orientation.

Looking at the heating behavior resulting from the different ply orientations as given in Figures 9 and 10, the following statements can be made:

- the shape of the heating pattern changes according to the ply orientations in the laminate
- solutions using the standard solver are only possible up to a UD layer cross-over angle of 50°
- solutions for laminates with cross-over ply orientations below 50° are possible with the new magnetostatic solver
- solutions for laminates with cross-over ply orientations below 50° give a very low heating effect

Parameter: $\hat{I}$ = 297,5 A; f = 490 KHz; V_f = 0,5; t_{Lam} = 2 mm; n_{UD} = 20; t = 1,17 s

25   **Temperature in °C**   90
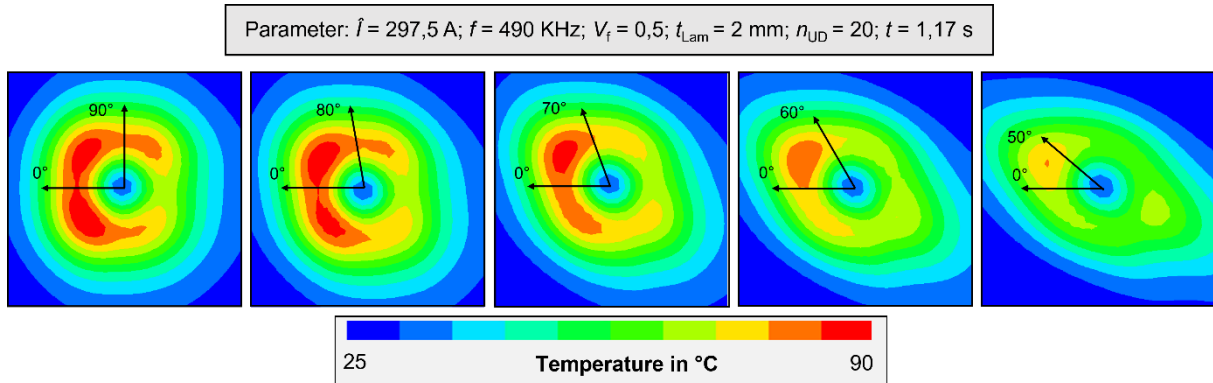
Fig.9:   Influence of ply orientation in the laminate on the resulting heating pattern on the backside of the laminate from [5].

Parameter: $\hat{I}$ = 297,5 A; f = 490 KHz; V_f = 0,5; t_{Lam} = 2 mm; n_{UD} = 20; t = 1,17 s

25   **Temperature in °C**   90
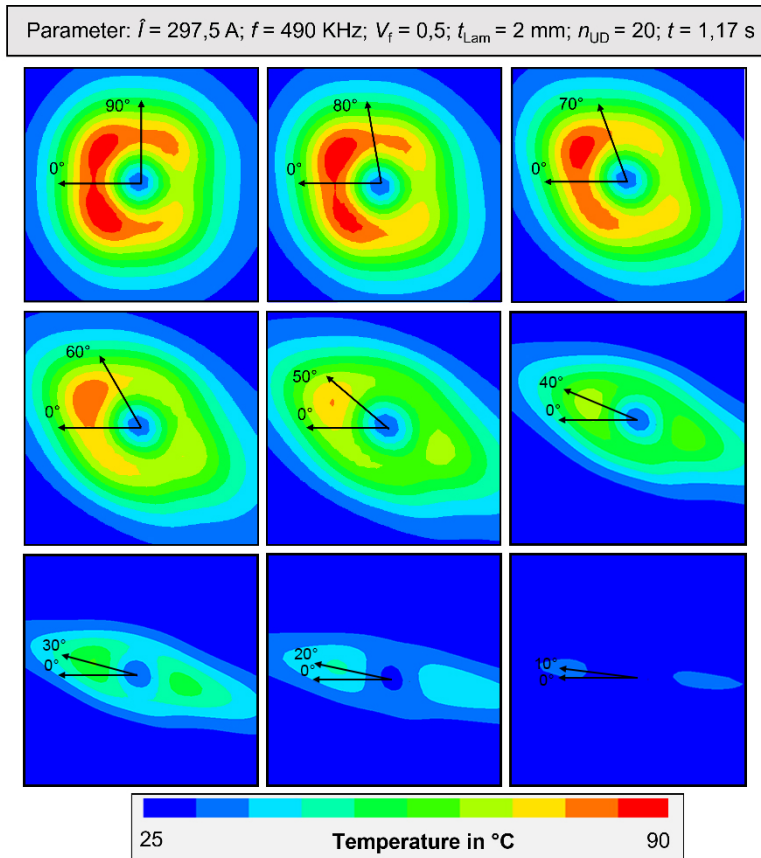
Fig.10: Influence of ply orientation in the laminate on the resulting heating pattern on the backside of the laminate using the new magnetostatic solver/ AMS preconditioner in LS-DYNA®.

Although no exact validations have been carried out for the simulation shown in Figures 9 and 10, a qualitative initial validation can be made using the work carried out by Grieser [9]. Here an experimental investigation of the heating behavior of two different laminate configurations produced from 3 mm thick carbon fiber polyetherketoneketone (CF-PEKK) laminates was carried out. A pancake inductor geometry was also used and thermal imaging on the back-side of the laminate was again used to visualize the resulting heating pattern. The two laminate configurations were [90°/0°/+-45°]$_6$ and [60°/30°/10°]$_8$. The results of the experimental heating tests are shown in Figure 11 showing a good qualitative agreement to the extreme influence on the resulting heating pattern caused by the laminate ply configuration using the same pancake inductor geometry. More concise validations in this respect is planned for future work.
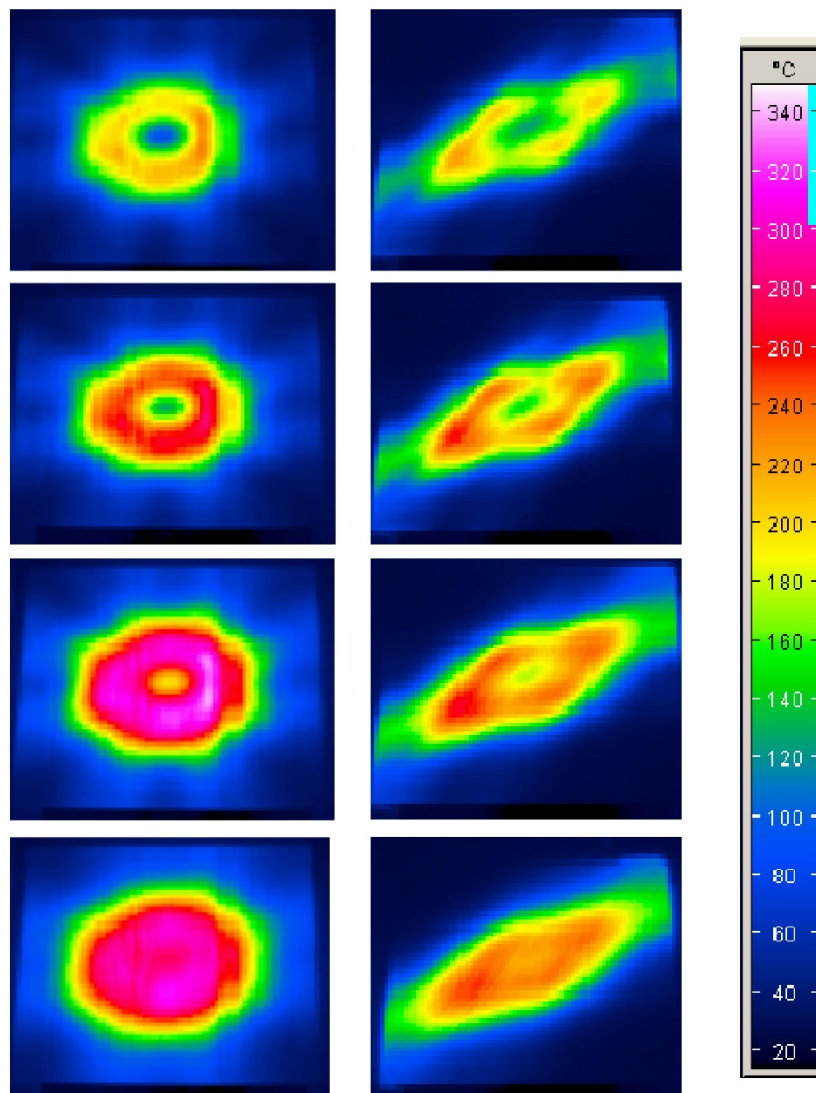
Fig.11: Temperature distribution of a 3mm thick [90°/0°/+-45°]$_6$ laminate (left) and a [60°/30°/10°]$_8$ laminate (right) with increasing heating time recorded with an infrared thermal camera [9].

4 Summary and conclusions

The investigations presented in this paper have shown that with the development of the material model described in [4] and the new magnetostatic solver implemented in LS-DYNA®, both qualitative and quantitative virtual investigations can be carried out in order to plan the correct inductor geometry and generator settings for a CFRTPC welding procedure. Future work will focus on the further enhancement of `*EM_MAT_002` (e.g. enabling BH curve input and directional magnetic permeability) and validation of the heating behavior prediction for various laminate configurations typically used in the aerospace industry. All the simulations shown in this paper have been carried out using the smp d version of LS-DYNA® R13-975-g4d2a4f8fdc.

5 Literature

[1]   Duhovic M., Moser L., Mitschang P., Maier M., Caldichoury I., L'Eplattenier P. Simulating the Joining of Composite Materials by Electromagnetic Induction. In Proceedings of the 12th International LS-DYNA® Users Conference, Electromagnetic (2), 3.-5. June, 2012, Detroit, USA. https://www.dynalook.com/conferences/12th-international-ls-dyna-conference/electromagnetic16-c.pdf

[2]   Duhovic M., Hümbert M., Mitschang P., Maier M., L'Eplattenier P., Caldichoury I. Further Advances in Simulating the Processing of Composite Materials by Electromagnetic Induction. In: Proceedings of the 13th International LS-DYNA® Users Conference, Electromagnetic, 8.-10.

June, 2014, Detroit, USA. https://www.dynalook.com/conferences/13th-international-ls-dyna-conference/electromagnetic/further-advances-in-simulating-the-processing-of-composite-materials-by-electromagnetic-induction

[3] Duhovic M., L'Eplattenier P., Caldichoury I., Mitschang P., Maier M. Advanced 3D Finite Element Simulation of Thermoplastic Carbon Fiber Composite Induction Welding. ECCM16 - 16th European Conference on Composite Materials, 22.-26. June, 2014, Seville, Spain.

[4] Hoffmann T., Becker S., Duhovic, M., Mitschang P. Simulating the Induction Heating Behavior of CFRTPC Laminates. In Proceedings of the 13th European LS-DYNA® Conference, 5.-7. October, 2021, Ulm/Online, Germany.

[5] Kielhorn L., Rüberg T., Zechner J. Robust FEM-BEM Coupling for LS-DYNA®'s EM module. In Proceedings of the 15th International LS-DYNA® Users Conference, Electromagnetics, 10.-12. June, 2018, Detroit, USA. https://www.dynalook.com/conferences/15th-international-ls-dyna-conference/electromagnetics/robust-fem-bem-coupling-for-ls-dyna-r-s-em-module

[6] https://fluxtrol.com/training-courses-Magnetic-Flux-Control [accessed on 27.08.2021].

[7] Khan MA. Experimental and Simulative Description of the Thermoplastic Tape Placement Process with Online Consolidation. Doctoral Thesis, Technische Universität Kaiserslautern, 2017. http://nbn-resolving.de/urn:nbn:de:hbz:386-kluedo-47293

[8] Moser L. Experimental Analysis and Modeling of Susceptorless Induction Welding of High Performance Thermoplastic Polymer Composites. Doctoral Thesis, Technische Universität Kaiserslautern, 2017. http://nbn-resolving.de/urn:nbn:de:hbz:386-kluedo-47404

[9] Grieser, T. Analysis of Inductive Heating of Carbon Reinforced High Performance Polymer Composites, Student Project Thesis, Technische Universität Kaiserslautern, 2009.